ARTICLES SCIENCE CHINA Materials

mater.scichina.com link.springer.com

Published online 4 April 2019 | https://doi.org/10.1007/s40843-019-9413-5
Sci China Mater 2019, 62(8): 1096–1104

Pt embedded Ni_3Se_2@NiOOH core-shell dendrite-like nanoarrays on nickel foam as bifunctional electrocatalysts for overall water splitting

Xuerong Zheng[1], Yanhui Cao[1], Xiaopeng Han[1], Hui Liu[2], Jihui Wang[1], Zhijia Zhang[3], Xianwen Wu[4], Cheng Zhong[1], Wenbin Hu[1] and Yida Deng[1*]

ABSTRACT **Developing high-performance bifunctional catalysts toward hydrogen evolution reaction (HER) and oxygen evolution reaction (OER) is essential to enhance water splitting efficiency for large-scale hydrogen production. Neither noble metal Pt nor transition metal compounds show satisfactory performances for both HER and OER simultaneously. Here, we prepared a three-dimensional Pt-Ni_3Se_2@NiOOH/NF (PNOF) hybrid catalyst *via in-situ* growth strategy. Benefitting from the self-supported structure and oxygen vacancies on the surface of NiOOH nanosheets, the PNOF electrode shows remarkably catalytic performance for dual HER and OER. The overall water electrolyzer using PNOF as anode and cathode can achieve a current density of 10 mA cm^{-2} at a low voltage of 1.52 V with excellent long-term stability, which is superior to precious metal catalysts of Pt/C and Ir/C. This study provides a promising strategy for preparing bifunctional catalysts with high performance.**

Keywords: Pt-Ni_3Se_2@NiOOH/NF, bifunctional catalyst, oxygen vacancy, overall water splitting

INTRODUCTION

Water electrolysis has been considered as a promising solution to the energy dilemma and environment pollution. It is critical to develop highly efficient and low cost bifunctional electrocatalysts to drive the half reactions of cathodic hydrogen evolution reaction (HER) and anodic oxygen evolution reaction (OER) [1–3]. Currently, precious metals Pt and Ir, as well as their alloys, are still the most efficient electrocatalysts for HER and OER. However, the high cost, terrestrial scarcity and non-bifunctional property impede their widespread utilization [4–6]. During the past decades, non-noble metal oxides, hydroxides, chalcogenides, phosphides and nitrides have attracted special attention as bifunctional catalysts for OER and HER due to their cost-competitiveness, high abundance and environmental friendliness [7–14]. Unfortunately, their electrochemical properties are still far away from that of noble metal catalysts due to the limited active sites and poor electrical conductivity. Constructing heterogeneous catalysts becomes one of the most valid issues to improve their catalytic activity and stability [5,15–17]. Recently, hybrid materials with the conjunction of transition metal oxides/hydroxides (TMO) and metal catalysts show great potential for electrocatalysis, due to the engineering surface electronic modulation arising from electron transfer between the fabricated nanointerfaces, thereby enhancing their catalytic performances [18–22].

Rational construction of Pt and TMO hybrid catalysts opens a highly promising way to improve the utilization efficiency and stability of precious metal. Pioneering studies have reported the fabrication of hybrid materials *via* combining Pt with $Ni(OH)_2$ [18,19], CoO [20], CeO_2 [21], $Ti_{0.7}Mo_{0.3}O_2$ [22], or $CaMnO_3$ [23], which exhibit enhanced catalytic activity and stability toward HER and OER. However, the construction of hybrid materials still faces some challenges. The active edge sites and in-

[1] School of Materials Science and Engineering, Key Laboratory of Advanced Ceramics and Machining Technology of Ministry of Education, Tianjin University, Tianjin 300072, China
[2] School of Materials Science and Engineering, Engineering Laboratory of Functional Optoelectronic Crystalline Materials of Hebei Province, Hebei University of Technology, Tianjin 300132, China
[3] School of Materials Science and Engineering, Tianjin Polytechnic University, Tianjin 300387, China
[4] School of Chemistry and Chemical Engineering, Jishou University, Jishou 416000, China
* Corresponding author (email: yida.deng@tju.edu.cn)

herently poor electric conductivity of TMO are the key problems for catalytic enhancement [24,25]. The synthesis of highly dispersed ultrathin TMO coupled with conductive substrate is still a challenge. Thus, tremendous efforts have focused on the improvement of active sites and conductivity of TMO catalysts [26,27]. Besides, the current hybrid materials are mainly in the form of particle agglomerates, which confines the chemisorption and desorption efficiency of reactants (H_2 and O_2) on the surface or interface of electrocatalysts [22,23]. Moreover, the perfect interfaces for hybrid catalysts possess strongly atomic and electronic coupling between heterogeneous domains. Thus, it is rather difficult to control the nucleation and growth of Pt on TMO surface precisely.

To overcome these issues, we designed and developed a dendrite-like core-shell structure Ni_3Se_2@NiOOH/NF (NOF) with Pt nanoparticles embedded in the ultrathin NiOOH nanosheets. Based on the experimental results, the designed catalysts are predicted with the following merits: 1) using nickel foam (NF) as Ni-precursor assures the high conductivity and electron transfer during electrochemical process; 2) the dendrite-like metallic Ni_3Se_2 arrays with vertical orientation results in enhanced electrochemical active surface area, which is favorable for mass transfer and bubble release; 3) the ultrathin NiOOH nanosheets with abundant oxygen vacancies, deriving from *in-situ* electrochemical oxidation, further increases the catalytic active sites. Consequently, such a PNOF hybrid catalyst demonstrates remarkable bifunctional electrocatalytic activities and durability compared with Ni_3Se_2@NiOOH/NF (NOF), Ni_3Se_2/NF benchmarks and even competes with the precious metal catalysts. Moreover, the integrated electrodes displayed an outstanding water splitting performance, with low overpotential of only 1.52 mV to achieve 10 mA cm^{-2}. Therefore, this work provides a promising strategy for preparing robust bifunctional catalysts for overall water splitting application.

EXPERIMENT

Materials synthesis (Ni_3Se_2/NF dendrite-like arrays, Ni_3Se_2@NiOOH/NF core-shell structure and Pt-Ni_3Se_2@NiOOH/NF catalyst)

Ni_3Se_2/NF dendrite-like arrays were synthesized by a facile polyols reduction selenization. The NF (1 cm×2 cm) was cleaned in acetone and ethanol thrice. Se powder (0.5 mmol) was dissolved in 30 mL trigthylene glycol (TEG) and then heated to 250°C. The NF was put into the hot Se solution and refluxing for 30 min. Then, the product was cooled to room temperature and then cleaned by sonication in ethanol for three times.

NOF core-shell structure was prepared by *in-situ* electrochemical reduction. Typically, it was performed on an electrochemical workstation at 1.6 V *versus* reversible hydrogen electrode (RHE) in 1.0 mol L^{-1} KOH for 8 h. Then the OER would happen on the surface of Ni_3Se_2 to form NiOOH nanosheets.

For the preparation of PNOF catalysts, *in-situ* polyols reduction was employed. Pt precursor was prepared by dissolving $H_2PtCl_6{\cdot}2H_2O$ (0.1 mmol) into deionized water (10 mL). The NOF was immersed into the Pt precursor at room temperature for 5 min and then heated at 60°C for 5 min, and the whole process was repeated for different cycles to load different amounts of Pt. For the *in-situ* reduction reaction, 20 mL ethylene glycol (EG) with 0.75 mmol KBr addition were heated to 180°C, and then the as-deposited Pt-precursor was immersed in the solution for 5 min for *in-situ* growth of Pt on the surface of NiOOH nanosheets. PNOF was cleaned by sonication in ethanol thrice.

Materials characterization

The crystalline structure of all products were analyzed by Bruker D8 Advanced X-ray diffractometer (XRD) with Cu Kα radiation at 6° min^{-1} from 2θ 10° to 90°. The surface morphology was observed by scanning electron microscope (FESEM, S-4800, Hitachi, Japan) and transition electron microscope (TEM, jem-2100f at 200 kV). The fast Fourier transform (FFT) was obtained from the corresponding HRTEM image. X-ray photoelectron spectroscopy (XPS) was measured on PerkinElmer PHI 1600 ESCA.

Electrocatalytic measurements

The OER and HER performances of the synthesized products were measured in 1.0 mol L^{-1} KOH aqueous solution with N_2 saturated, using a graphite rod as counter electrode, a saturated calomel electrode (SCE) as reference electrode, and the catalysts as the working electrode. The linear sweeping voltammetry (LSV) was measured with a scan rate of 5 mV s^{-1} and corrected with the equation of *iR*-compensation: $E_c = E_m - I_m \times R_s$, with E_c, E_m, I_m, and R_s standing for compensated voltage, measured voltage, measured current, and electrolyte resistance, respectively. The potentials in this paper were transferred to the RHE with equation: $E_{vsRHE} = E_{vsSCE} + 1.067$ V in 1.0 mol L^{-1} KOH. The Nyquist plots of electrochemical impedance spectra (EIS) were measured with a frequency ranging from 10 kHz to 0.1 Hz. To evaluate

the effective electrochemical active surface areas (ECSA), the electrochemical capacitance (C_{dl}) parameters were tested from 1.067 to 1.167 V by cyclic voltammetry (CVs) curves at scanning rate of 3, 5, 8, 10, 15, 20, 30, 50, 70 and 100 mV s^{-1} respectively. The overall water-splitting test was carried out in N_2-saturated 1.0 mol L^{-1} KOH electrolyte at 5 mV s^{-1} using Pt-Ni_3Se_2@NiOOH/NF as the anode and cathode.

RESULTS AND DISCUSSION

For the preparation of PNOF hybrid catalysts (Fig. S1), three dimensional NF catalysts were employed as support. In the fabrication process, the tunable Ni_3Se_2 dendrite-like arrays were first *in-situ* fabricated in Se solution at high temperature with NF as Ni resource (Fig. 1a, b and Fig. S1). Then, ultrathin NiOOH nanosheets were *in-situ* derived from the surface of Ni_3Se_2 by electrochemical oxidation at 1.6 V *versus* RHE (Fig. 1c). Furthermore, Pt was deposited on the surface of NiOOH nanosheets with controlled deposition cycles, followed by *in-situ* reduction to achieve Pt nanoparticles in ethylene glycol at 180°C for 5 min (Fig. 1d, e). Notably, the loading mass of Pt nanoparticles can be well-controlled by tuning the deposition cycles (Fig. S2, see details in the experimental section). The energy dispersive X-ray spectroscopy (EDS) and inductively coupled plasma mass spectrometry (ICP-MS) were performed to identify the loading mass of Pt (Table S1). For depositing 4 cycles, the small Pt nanoparticles distribute homogenously on the surface of bulk face with the loading mass of 8.2 wt%. However, lower mass loading of Pt (2.5 wt%) results in an uneven distribution, while higher mass loading (15.6 wt%) leads to larger size and agglomeration of Pt nanoparticles. Therefore, we select PNOF hybrid with Pt content of 8.2 wt% for further study. The coexistence of Se and O in the EDS (Fig. S2) indicates that Ni_3Se_2 was partly oxidized into NiOOH on the surface of Ni_3Se_2/NF, thus leading to the core-shell Ni_3Se_2@NiOOH. Moreover, the fabrication of PNOF hybrid catalysts is size-controllable (Fig. S3) and it is meaningful for the practical application.

For XRD analysis, the products were sonicated and centrifuged adequately to obtain powder products. The XRD pattern of Ni_3Se_2/NF (Fig. 2a) demonstrates that all the diffraction peaks can be indexed to the hexagonal Ni_3Se_2 (JCPDS No. 19-0841) which has been identified to be a high-efficient OER catalyst with extended stability [28]. The atomic ratio of Ni:Se in Ni_3Se_2 is in accordance with the result of EDS (Fig. S4). Compared with the XRD pattern of Ni_3Se_2/NF, the diffraction peaks at positions of 28.2°, 37.6° and 42.3° for NOF confirmed the NiOOH

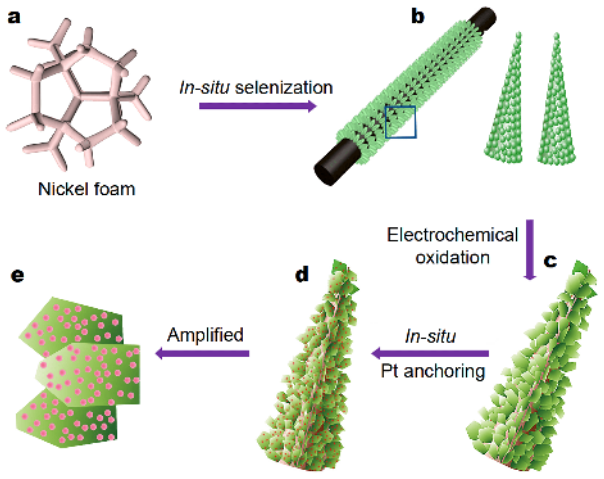

Figure 1 Schematic illustration for the synthesis of three dimensional PNOF nanohybrids. (a) NF cleaned by sonication in acetone and ethanol for at least 30 min. (b) *In-situ* fabrication of Ni_3Se_2 dendrite-like arrays by directly selenization assisted with polyols. (c) *In-situ* electrochemical oxidation to prepare NOF core-shell structure. (d) *In-situ* growth of Pt nanoparticles anchoring on the surface of NOF. (e) The amplified Pt/NiOOH structure.

(JCPDS No. 27-0956) with poor crystallinity, similar to the previous report about Ni-based system [29]. As shown in Fig. 2b, the well-controlled dendrite-like Ni_3Se_2 arrays directly grow on the conductive NF. This structure provides a direct pathway for charge transfer and bubble release during the electrochemical processes, which is essential to enhance the catalytic activity. The TEM image (inset of Fig. 2c) demonstrates that the dendrite-shaped Ni_3Se_2 vertically disperse on the trunk as several polyhedronal nanocrystals randomly with the lattice distance of 0.291 nm corresponding to the (012) plane of hexagonal Ni_3Se_2 (Fig. 2c), consistent with the XRD analysis.

The SEM, TEM and HRTEM images (Fig. 2d, e and Fig. S5) of the scratched Ni_3Se_2@NiOOH on NOF confirm its core-shell structure after *in-situ* electrochemical oxidation. The inner Ni_3Se_2 is wrapped by ultrathin outer shell NiOOH nanosheets (Fig. 2d). The HRTEM image reveals the interface between Ni_3Se_2 and NiOOH (Fig. 2e). The lattice distance of 0.21 nm corresponds to the (103) facet of NiOOH with poor crystallinity, which is in accordance with the previous reports on the similar materials [30,31]. For further investigation, electron spin resonance (ESR) spectra (Fig. 2f) were applied to investigate the oxygen vacancies in Ni_3Se_2/NF and NOF [32–35]. The high intensity in the ESR spectrum represents high concentration of oxygen vacancies [32]. Negligible ESR signal is in Ni_3Se_2/NF, indicating the absence of oxygen vacancy. However, NOF shows strongly

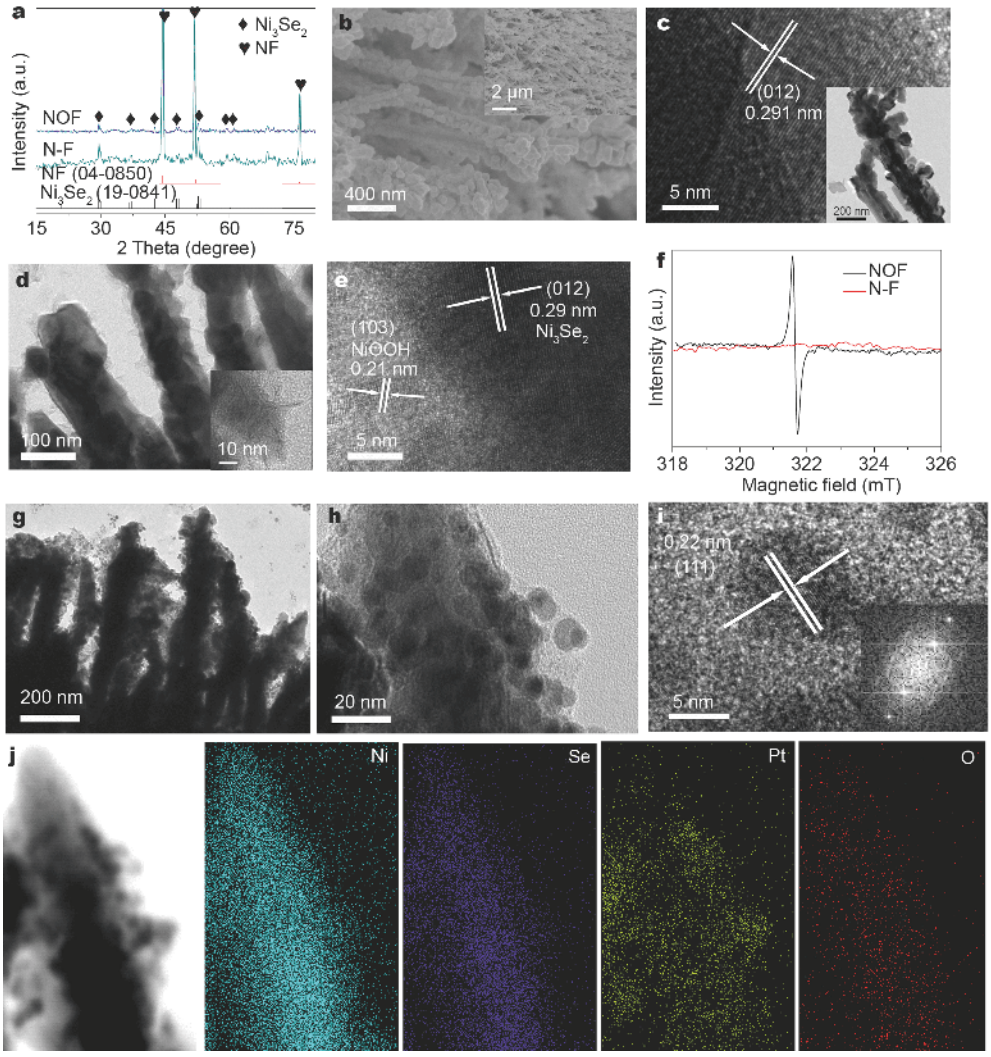

Figure 2 (a) XRD patterns of Ni_3Se_2/NF and NOF catalysts, SEM and low-magnification SEM (inset) images (b) and HRTEM and TEM (inset) images (c) of Ni_3Se_2/NF. (d) TEM and enlarged TEM (inset) images of core-shell NOF. (e) HRTEM image of Ni_3Se_2@NiOOH with an obvious interface. (f) The room-temperature ESR spectra of NOF and Ni_3Se_2/NF. TEM image (g) and high magnification TEM image (h) of PNOF. (i) HRTEM image of Pt nanoparticles embedded on the surface of NiOOH nanosheets, and the corresponding FFT patterns (inset) of Pt nanoparticles. (j) TEM image and EDX elemental mapping of Ni, Se, Pt and O in PNOF hybrid catalysts.

oxygen vacancy-related ESR signal at the same position as the related reports [24]. This phenomenon demonstrates that the *in-situ* electrochemical treatment can induce more unpaired electrons trapped on the oxygen-vacancy sites and therefore more oxygen vacancies appear on the surface of Ni_3Se_2/NF [33]. It is easy for surface oxygen vacancies to adsorb O_2 and convert into active oxygen species O^{2-}, with the ESR signal at 321.7 mT [34]. Amount of "V_O" formed on the surface of NiOOH nanosheets is favorable to provide active sites and enhance the catalytic performances [24,36,37]. The oxygen vacancy may derive from the reduction of Ni during electrochemical oxidation and the oxygen in Ni–O bonds which could be oxidized into O_2 during OER process [38,39].

For PNOF hybrid catalysts with Pt mass loading of 8.2 wt%, SEM and TEM images (Fig. 2g, h and Fig. S6) show that Pt nanoparticles with crystal size of 5–10 nm are uniformly anchored on the surface of NiOOH nanosheets. The identified lattice space of 0.22 nm corresponds to the (111) of Pt, which is the most active plane for HER catalysis [20]. According to the EDX elemental mapping of PNOF with four deposition cycles (Fig. 2j), the Ni (cyan), Se (purple), Pt (yellow) and O (red) dis-

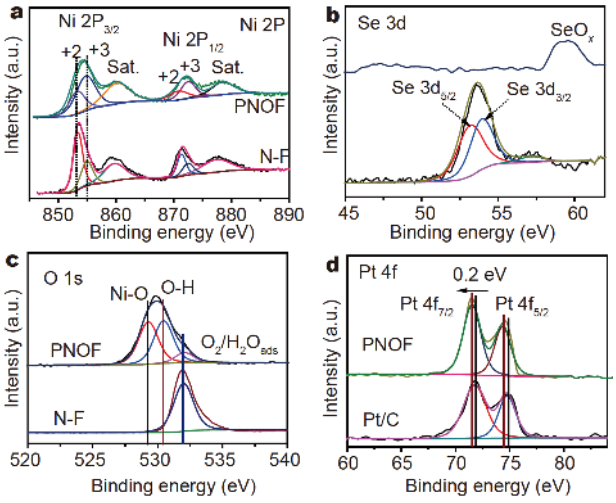

Figure 3 XPS spectra of (a) Ni 2p for Ni_3Se_2/NF and PNOF catalysts, (b) Se 3d for Ni_3Se_2/NF and NOF catalysts, (c) O 1s for Ni_3Se_2/NF and NOF catalysts, (d) Pt 4f for PNOF and 20 wt% Pt/C catalysts.

tribute homogeneously.

XPS was employed to investigate not only the chemical states of Pt, NiOOH and Ni_3Se_2, but also the electronic interaction between them. The XPS survey spectrum (Fig. S7) confirms the existence of Ni, Pt, Se, C and O elements. As shown in Fig. 3a, the Ni $2p_{3/2}$ peak shifts from 853.1 eV in Ni_3Se_2/NF to 854.8 eV in PNOF hybrids. Notably, the increase of Ni^{3+} and decrease of Ni^{2+} in NOF indicates the appearance of NiOOH on the surface of catalyst. As reported, the increase of the higher valence state of Ni^{3+} sites is beneficial to electrocatalytic property because it is prior to the onset of oxygen evolution [40]. Moreover, the reduction of electron density around Ni can provide more empty d orbits and thus enhance binding with H atoms, facilitating the kinetics and contributing to smaller Tafel slope and higher HER and OER activity [5]. In Fig. 3b, the Se 3d peaks nearly vanish and only SeO_x left on the surface of NOF, indicating the surface oxidation of Ni_3Se_2 into NiOOH nanosheets. Due to the limited penetration depth of XPS (2–3 nm), NiOOH shell cannot be penetrated completely, thus the Ni_3Se_2 core cannot be detected. As shown in Fig. 3c, the peaks at 530.5, 531.4 and 532.5 eV can be attributed to Ni–O, O–H and the adsorbed H_2O or O_2, respectively. Compared with pure phase Ni_3Se_2, the strong peaks of O 1s at 530.5 and 531.4 eV confirmed NiOOH as the main species on the surface of NOF. The peaks located at 71.4 and 74.3 eV in PNOF catalysts are assigned to Pt $4f_{7/2}$ and Pt $4f_{5/2}$, respectively (Fig. 3d). Both peaks of Pt in PNOF slightly shift towards lower binding energy compared with that of Pt/C, which may be caused by the strongly coupling interaction between NiOOH and Pt [22,41]. Notably, the coupling interaction and interfacial synergy between Pt and bulk phase is favorable for the acceleration of the kinetic process for OER and HER catalysis, thus optimizing the electrocatalytic properties [20,22,41]. These results suggest that the PNOF hybrid catalyst has potential application in electrochemical catalysis.

The HER and OER activities of PNOF as an efficient bifunctional electrocatalyst were investigated (Fig. 4 and Table S2). Compared with other catalysts, PNOF exhibits high HER performance with an overpotential of 46 mV for delivering a current density of 10 mA cm^{-2}, which is equal to the state-of-the-art 20 wt% Pt/C catalyst. Impressively, the HER current density of PNOF surpassed that of benchmark Pt/C catalyst at high potential (more negative than 100 mV). The overpotentials of NOF, Ni_3Se_2/NF and NF were 95, 131 and 337 mV higher than that of PNOF at 10 mA cm^{-2}, respectively. The PNOF catalyst is one of the most highly efficient catalysts for HER performance as recent reports (Table S3). Moreover, the PNOF catalyst shows a corresponding HER Tafel slope of 45 mV dec^{-1}, which is comparable with benchmark Pt/C catalyst and much smaller than other catalysts (Fig. 4b). Generally, the smaller Tafel slope indicates faster kinetics for HER catalysis and more rapid increase in the rate of H_2 generation with the applied overpotential, confirmed by the polarization curves. Based on the classic theory [5,41], mainly two steps involved in the HER process. Firstly, Volmer reaction is a discharge step and corresponding to Tafel slope of 118 mV dec^{-1}, as Equation (1):

$$H_2O + e^- + M \rightleftarrows M\text{-}H_{ads} + OH^-. \quad (1)$$

M is the surface active site, and H_{ads} is the adsorbed hydrogen. Secondly, Heyrovsky reaction is ion or atom reaction with a slope of 40 mV dec^{-1}, which is in accordance with that of PNOF catalyst and expressed as Equation (2):

$$M\text{-}H_{ads} + H_2O + e^- \rightleftarrows H_2 + OH^-. \quad (2)$$

Although the Tafel slope could not determine the specific mechanism sufficiently, the much smaller value for PNOF (45 mV dec^{-1}) compared with other benchmarks confirms the enhanced Volmer step in HER kinetics. Moreover, related reports also confirm that the nickel-based chalcogenides (such as NiS) can promote water dissociation substantially and thus increase the rate of H_{ads} formation [42].

In addition, the mass activity ($J_{k,\,mass}$) of PNOF hybrid

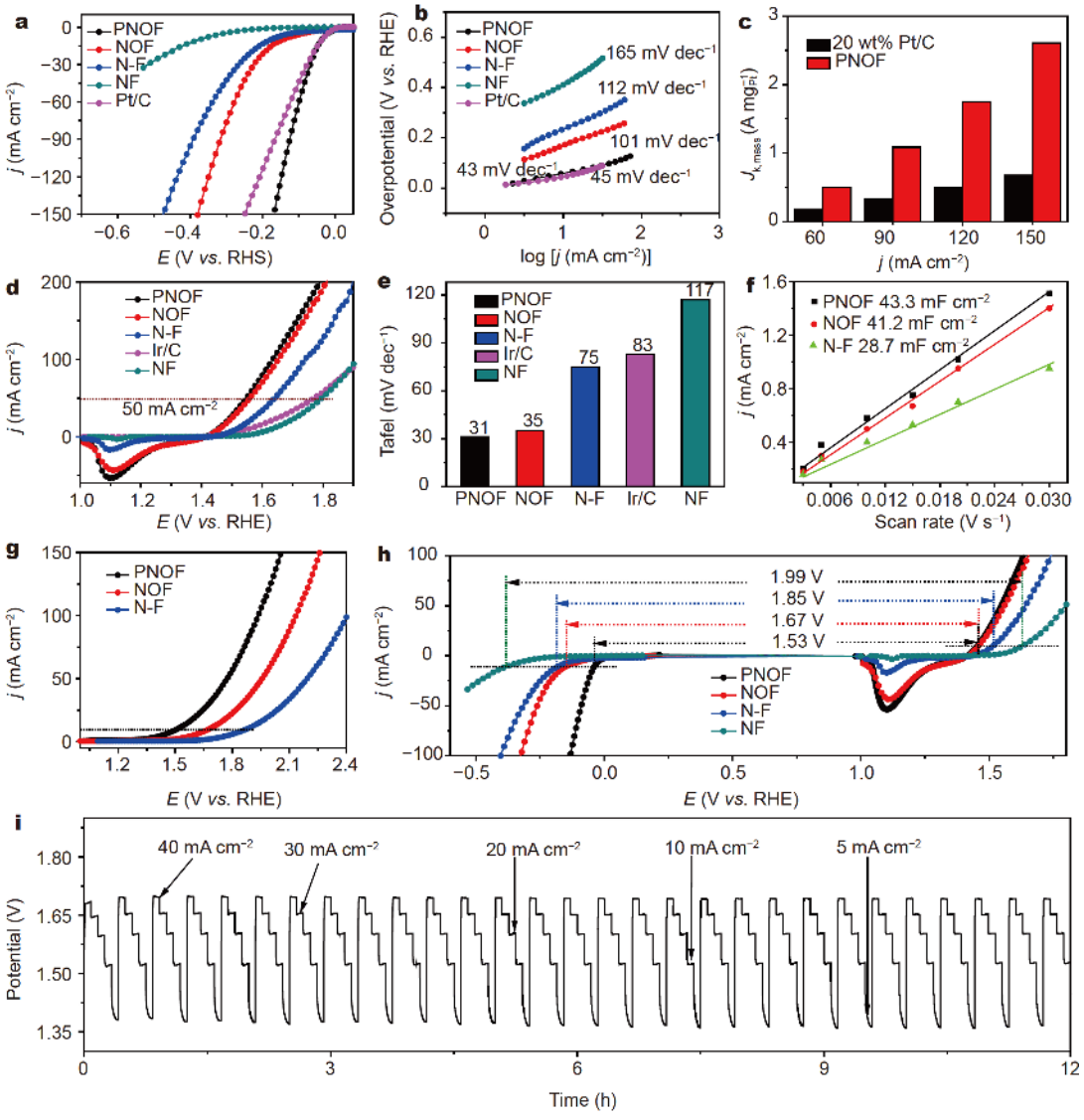

Figure 4 (a) HER polarization curves of PNOF, NOF, Ni_3Se_2/NF, NF and Pt/C catalysts at a scan rate of 5 mV s^{-1} in 1.0 mol L^{-1} KOH. (b) Corresponding HER Tafel plots. (c) Mass activity ($J_{k,mass}$) of PNOF hybrid catalysts in comparison with 20 wt% Pt/C at different current densities. (d) OER polarization curves of PNOF, NOF, Ni_3Se_2/NF, NF and Pt/C catalysts at a scan rate of 5 mV s^{-1} in 1.0 mol L^{-1} KOH. (e) Corresponding OER Tafel plots. (f) Dependence of current densities as a function of scan rates. (g) Polarization curves of PNOF, NOF and Ni_3Se_2/NF for overall alkaline water splitting in a two-electrode configuration. (h) ΔE calculated from the polarization curves of PNOF, NOF, Ni_3Se_2/NF and NF for HER and OER from Fig. 4a and d. (i) Cycling stability of PNOF for water electrolysis in 1.0 mol L^{-1} KOH with different current densities.

catalysts is about 3.2 times higher than that of Pt/C, indicating the high intrinsic electrochemical activity for HER catalysis (Fig. 4c). This result indicates that the enclosed Pt nanoparticles plays a key role in enhancing the HER activity. Besides, the superior performance of PNOF may be also attributed to the perfect electronic coupling between Pt and NiOOH nanosheets, which has been confirmed [5]. The HER performances of PNOF with different Pt contents were also evaluated (Fig. S8). The HER activities first improve with the increasing Pt mass loading and then decrease from 15.6 wt% of Pt. The activity trend can be attributed to the decrease of active sites at less mass loading and large size and agglomeration of Pt nanoparticles at higher mass loading. For practical application, the cycle stability of PNOF electrode was also tested (Fig. S9). The well repeated LSV curves (before and after 1,000 cycles) for PNOF demonstrate a remarkable long-term durability for HER electrocatalysis.

At the same time, the OER polarization curves were also recorded in N_2 saturated 1.0 mol L^{-1} KOH with a scan rate of 5 mV s^{-1} (Fig. 4d). Obviously, PNOF electrode shows a small overpotential of 310 mV to achieve a current density of 50 mA cm^{-2}, which is 10, 90, 230, and 200 mV smaller than that of NOF, Ni_3Se_2/NF, NF and Ir/C, respectively. The redox peak at 1.15 V *vs.* RHE for Ni-based catalysts is attributed to the Ni^{2+}/Ni^{3+} couple [26,43]. Based on the OER performance, PNOF is one the most active catalysts (Table S4). Similarly, the lowest OER Tafel slope of PNOF demonstrates an appreciable kinetics for OER catalysis (Fig. 4e and Fig. S10). Meanwhile, Nyquist plots of EIS (Fig. S11) are well in accordance with the trend of LSV for OER, further proving the enhanced conductivity for electrocatalytic performances. The OER performance of PNOF catalysts with different Pt contents were also evaluated (Fig. S12) and exhibited the same activity trend as that of HER. In addition, the double layer capacitance (C_{dl}) was characterized to calculate the ECSA of PNOF, NOF and Ni_3Se_2/NF catalysts (Fig. 4f and Fig. S13). The C_{dl} of PNOF catalyst was 50% higher than that of Ni_3Se_2/NF, indicating higher intrinsic catalytic activity associated with Pt-NiOOH-Ni_3Se_2 synergy.

Moreover, the OER cycle stability of PNOF electrode was tested. The well repeated LSV curves for PNOF demonstrate a remarkable long-term durability for OER electrocatalysis (Fig. S14). The morphology and crystal structure of NOF and PNOF after 1,000 OER cycles were characterized (Fig. S15). Interestingly, TEM images show that the surface of NiOOH nanosheets on the PNOF catalyst (Fig. S15b, c) is more visible than that of NOF (Fig. S15a) after the same OER process. Besides, the increased diffraction peaks of NiOOH in powder XRD (Fig. S15d) suggest the increase of out-layer for PNOF catalyst after OER catalysis. The collected results demonstrate that the NiOOH nanosheets prefer to generate on PNOF catalyst surface possibly attributed to the modified electronic configuration of Ni species by Pt deposition. As the real catalytically active sites toward OER, these oxide species play a key role for the remarkable OER activity of PNOF catalyst.

Generally, the optimal HER and OER performance may be attributed to the formation of Ni_3Se_2/NiOOH core-shell structure and the synergetic catalytic action between Pt, Ni_3Se_2 core and NiOOH shell. The *in-situ* hydroxide species NiOOH formed under oxidizing potential acts as the real catalytically active sites toward OER process, and the enclosed Pt further increases the oxidation degree of NiOOH during OER process. The considerable conductivity of Ni_2Se_3 also contributes to the superior catalytic activity by offering efficient electron transfer for the OER active oxide layer. As for HER, the homogeneous distribution of ultrafine Pt nanoparticles and positive synergistic interaction between Pt and NiOOH nanosheets accelerate the rate of water dissociation and hydrogen adsorption, enhancing the electrocatalytic HER activity and stability [44]. Therefore, the ideal HER and OER performances of PNOF are associated with not only the abundant active sites, but also the high catalysis kinetics.

For energy conversion application, PNOF, NOF and Ni_3Se_2/NF were installed as bifunctional catalysts in overall water splitting devices in 1.0 mol L^{-1} KOH (Fig. S16). All the electrodes were employed as both anode and cathode directly. According to the polarization curves (Fig. 4g), the electrolyzers provide a current density of 10 mA cm^{-2} at 1.52, 1.67 and 1.87 V for PNOF, NOF and Ni_3Se_2/NF, respectively (Table S2). Notably, PNOF exhibits superior water splitting performance to those of NOF and Ni_3Se_2/NF, confirming that the synergy effect between Pt, NiOOH and Ni_3Se_2 is efficient for overall water splitting. Theoretically, the potential difference (ΔV) between OER and HER should be in accordance with the voltage for water splitting at the same current density. The calculated ΔV for PNOF, NOF and Ni_3Se_2/NF were 1.53, 1.67 and 1.85 V, respectively, almost identical to the performances in water splitting devices at a current density of 10 mA cm^{-2} (Fig. 4h). The performance of PNOF for overall water splitting is comparable with that of recently reported catalysts in similar condition (Table S5). The Faradaic efficiency of the PNOF electrodes for water splitting was evaluated by comparing the experimentally generated volume of gas with the theoretical values (Fig. S17). Obviously, the molar ratio of H_2 and O_2 is 2:1, and the measured gas volume is in accordance with the calculated volume, indicating a Faradaic efficiency of nearly 100%. To investigate the durability of PNOF in practical application, a novel experiment was carried out by applying current density of 5, 10, 20, 30 and 40 mA cm^{-2} with 1,500 s for one cycle and repeated for 12 h with no obvious active decay, indicating the remarkable stability of PNOF for water splitting (Fig. 4i). These collective results suggested the promising application of PNOF catalyst in overall water splitting devices as bifunctional catalyst.

CONCLUSIONS

In conclusion, we demonstrate an *in-situ* strategy for preparing core-shell structure NOF with Pt nanoparticles embedded on the surface of dendrite-like arrays. Bene-

fitting from the rational design of dendrite hybrid structure, PNOF electrode exhibits fascinating HER and OER performances, and achieves a current density of 10 mA cm^{-2} at a voltage of only 1.52 V for overall water splitting. The excellent catalytic activity and remarkable stability of PNOF can be attributed to the abundant active sites, highly electronic conductivity, amount of oxygen vacancies and synergistic catalytic effect. Therefore, the *in-situ* growth for selenization, electrochemical oxidation and Pt anchoring provides a promising strategy for constructing efficient bifunctional electrocatalysts.

Received 25 January 2019; accepted 11 March 2019; published online 4 April 2019

1 Singh S, Jain S, Ps V, *et al.* Hydrogen: A sustainable fuel for future of the transport sector. Renew Sustain Energy Rev, 2015, 51: 623–633
2 Wang P, Jiang K, Wang G, *et al.* Phase and interface engineering of platinum-nickel nanowires for efficient electrochemical hydrogen evolution. Angew Chem Int Ed, 2016, 55: 12859–12863
3 Zhang X, Shao J, Huang W, *et al.* Three dimensional carbon substrate materials for electrolysis of water. Sci China Mater, 2018, 61: 1143–1153
4 Zhang Y, Zhang J, Chen Z, *et al.* One-step synthesis of the PdPt bimetallic nanodendrites with controllable composition for methanol oxidation reaction. Sci China Mater, 2018, 61: 697–706
5 Wang P, Zhang X, Zhang J, *et al.* Precise tuning in platinum-nickel/nickel sulfide interface nanowires for synergistic hydrogen evolution catalysis. Nat Commun, 2017, 8: 14580
6 Zou X, Zhang Y. Noble metal-free hydrogen evolution catalysts for water splitting. Chem Soc Rev, 2015, 44: 5148–5180
7 Liu X, Liu W, Ko M, *et al.* Metal (Ni, Co)-metal oxides/graphene nanocomposites as multifunctional electrocatalysts. Adv Funct Mater, 2015, 25: 5799–5808
8 Zheng X, Zhang Y, Liu H, *et al. In situ* fabrication of heterostructure on nickel foam with tuned composition for enhancing water-splitting performance. Small, 2018, 14: 1803666
9 Zheng X, Han X, Liu H, *et al.* Controllable synthesis of Ni_xSe ($0.5 \leq x \leq 1$) nanocrystals for efficient rechargeable zinc-air batteries and water splitting. ACS Appl Mater Interfaces, 2018, 10: 13675–13684
10 Li Y, Liu B, Wang H, *et al.* Co_3O_4 nanosheet-built hollow dodecahedrons *via* a two-step self-templated method and their multifunctional applications. Sci China Mater, 2018, 61: 1575–1586
11 Zhang Z, Liu G, Cui X, *et al.* Crystal phase and architecture engineering of lotus-thalamus-shaped Pt-Ni anisotropic superstructures for highly efficient electrochemical hydrogen evolution. Adv Mater, 2018, 30: 1801741
12 Deng J, Deng D, Bao X. Robust catalysis on 2D materials encapsulating metals: concept, application, and perspective. Adv Mater, 2017, 29: 1606967
13 Ling T, Yan DY, Wang H, *et al.* Activating cobalt(II) oxide nanorods for efficient electrocatalysis by strain engineering. Nat Commun, 2017, 8: 1509
14 Zhang FS, Wang JW, Luo J, *et al.* Extraction of nickel from NiFe-LDH into Ni_2P@NiFe hydroxide as a bifunctional electrocatalyst for efficient overall water splitting. Chem Sci, 2018, 9: 1375–1384
15 Meng C, Ling T, Ma TY, *et al.* Atomically and electronically coupled Pt and CoO hybrid nanocatalysts for enhanced electrocatalytic performance. Adv Mater, 2017, 29: 1604607
16 Zhang J, Chen J, Luo Y, *et al.* Controllable synthesis of two-dimensional tungsten nitride nanosheets as electrocatalysts for oxygen reduction reaction. Sci China Mater, 2018, 61: 1567–1574
17 An L, Li Y, Luo M, *et al.* Atomic-level coupled interfaces and lattice distortion on CuS/NiS_2 nanocrystals boost oxygen catalysis for flexible Zn-air batteries. Adv Funct Mater, 2017, 27: 1703779
18 Subbaraman R, Tripkovic D, Strmcnik D, *et al.* Enhancing hydrogen evolution activity in water splitting by tailoring Li^+-$Ni(OH)_2$-Pt interfaces. Science, 2011, 334: 1256–1260
19 Yin H, Zhao S, Zhao K, *et al.* Ultrathin platinum nanowires grown on single-layered nickel hydroxide with high hydrogen evolution activity. Nat Commun, 2015, 6: 6430
20 Dou J, Tang Y, Nie L, *et al.* Complete oxidation of methane on Co_3O_4/CeO_2 nanocomposite: A synergic effect. Catal Today, 2018, 311: 48–55
21 Vayssilov GN, Lykhach Y, Migani A, *et al.* Support nanostructure boosts oxygen transfer to catalytically active platinum nanoparticles. Nat Mater, 2011, 10: 310–315
22 Ho VTT, Pan CJ, Rick J, *et al.* Nanostructured $Ti_{0.7}Mo_{0.3}O_2$ support enhances electron transfer to Pt: High-performance catalyst for oxygen reduction reaction. J Am Chem Soc, 2011, 133: 11716–11724
23 Han X, Cheng F, Zhang T, *et al.* Hydrogenated uniform Pt clusters supported on porous $CaMnO_3$ as a bifunctional electrocatalyst for enhanced oxygen reduction and evolution. Adv Mater, 2014, 26: 2047–2051
24 Yin J, Li Y, Lv F, *et al.* Oxygen vacancies dominated NiS_2/CoS_2 interface porous nanowires for portable Zn-air batteries driven water splitting devices. Adv Mater, 2017, 29: 1704681
25 Dutta S, Indra A, Feng Y, *et al.* Self-supported nickel iron layered double hydroxide-nickel selenide electrocatalyst for superior water splitting activity. ACS Appl Mater Interfaces, 2017, 9: 33766–33774
26 Li X, Han GQ, Liu YR, *et al.* NiSe@NiOOH core–shell hyacinth-like nanostructures on nickel foam synthesized by *in situ* electrochemical oxidation as an efficient electrocatalyst for the oxygen evolution reaction. ACS Appl Mater Interfaces, 2016, 8: 20057–20066
27 Han X, He G, He Y, *et al.* Engineering catalytic active sites on cobalt oxide surface for enhanced oxygen electrocatalysis. Adv Energy Mater, 2018, 8: 1702222
28 Swesi AT, Masud J, Nath M. Nickel selenide as a high-efficiency catalyst for oxygen evolution reaction. Energy Environ Sci, 2016, 9: 1771–1782
29 Zhang Q, Zhang C, Liang J, *et al.* Orthorhombic α-NiOOH nanosheet arrays: Phase conversion and efficient bifunctional electrocatalysts for full water splitting. ACS Sustain Chem Eng, 2017, 5: 3808–3818
30 Trotochaud L, Young SL, Ranney JK, *et al.* Nickel–iron oxyhydroxide oxygen-evolution electrocatalysts: The role of intentional and incidental iron incorporation. J Am Chem Soc, 2014, 136: 6744–6753
31 Sun H, Xu X, Yan Z, *et al.* Porous multishelled Ni_2P hollow microspheres as an active electrocatalyst for hydrogen and oxygen evolution. Chem Mater, 2017, 29: 8539–8547
32 Shi C, Liu J, Li W, *et al.* Hydrogen plasma reduction induced oxygen vacancies in cubic In_2O_3 particles with enhanced photocatalytic performance. Ceramics Int, 2018, 44: 22235–22240

33 Nakamura I, Negishi N, Kutsuna S, *et al.* Role of oxygen vacancy in the plasma-treated TiO_2 photocatalyst with visible light activity for NO removal. J Mol Catal A-Chem, 2000, 161: 205–212
34 Wang D, Shen H, Guo L, *et al.* Ag/Bi_2MoO_{6-x} with enhanced visible-light-responsive photocatalytic activities *via* the synergistic effect of surface oxygen vacancies and surface plasmon. Appl Surf Sci, 2018, 436: 536–547
35 Wang Y, Cao H, Chen L, *et al.* Tailored synthesis of active reduced graphene oxides from waste graphite: Structural defects and pollutant-dependent reactive radicals in aqueous organics decontamination. Appl Catal B-Environ, 2018, 229: 71–80
36 Bao J, Zhang X, Fan B, *et al.* Ultrathin spinel-structured nanosheets rich in oxygen deficiencies for enhanced electrocatalytic water oxidation. Angew Chem Int Ed, 2015, 54: 7399–7404
37 Lei F, Sun Y, Liu K, *et al.* Oxygen vacancies confined in ultrathin indium oxide porous sheets for promoted visible-light water splitting. J Am Chem Soc, 2014, 136: 6826–6829
38 Grimaud A, Diaz-Morales O, Han B, *et al.* Activating lattice oxygen redox reactions in metal oxides to catalyse oxygen evolution. Nat Chem, 2017, 9: 457–465
39 Lu X, Wang G, Zhai T, *et al.* Stabilized TiN nanowire arrays for high-performance and flexible supercapacitors. Nano Lett, 2012, 12: 5376–5381
40 Chen GF, Ma TY, Liu ZQ, *et al.* Efficient and stable bifunctional electrocatalysts Ni/Ni_xM_y (M = P, S) for overall water splitting. Adv Funct Mater, 2016, 26: 3314–3323
41 Han X, Wu X, Deng Y, *et al.* Ultrafine Pt nanoparticle-decorated pyrite-type CoS_2 nanosheet arrays coated on carbon cloth as a bifunctional electrode for overall water splitting. Adv Energy Mater, 2018, 8: 1800935
42 Yang Y, Zhang K, Lin H, *et al.* MoS_2-Ni_3S_2 heteronanorods as efficient and stable bifunctional electrocatalysts for overall water splitting. ACS Catal, 2017, 7: 2357–2366
43 Xu K, Ding H, Jia K, *et al.* Solution-liquid-solid synthesis of hexagonal nickel selenide nanowire arrays with a nonmetal catalyst. Angew Chem Int Ed, 2016, 55: 1710–1713
44 Xing Z, Han C, Wang D, *et al.* Ultrafine Pt nanoparticle-decorated $Co(OH)_2$ nanosheet arrays with enhanced catalytic activity toward hydrogen evolution. ACS Catal, 2017, 7: 7131–7135

Acknowledgements This work was supported by the National Natural Science Foundation of China (51804216, 51472178 and U1601216), Tianjin Natural Science Foundation (16JCYBJC17600) and Shen-zhen Science and Technology Foundation (JCYJ20170307145703486). The authors would also like to express gratitude to Ms. Jinfeng Zhang and Ms. Jing Mao for their assistance in TEM and EDS analysis, respectively.

Author contributions Zheng X and Hu W designed and engineered the samples; Cao Y and Han X performed the experiments; Liu H, Wang J and Zhong C performed the data analysis; Zhang Z and Wu X helped analyze the results; Zheng X and Deng Y wrote the manuscript. All authors contributed to the general discussion.

Conflict of interest The authors declare no competing financial interest.

Supplementary information EDS, SEM and TEM images of PNOF, NOF and Ni_3Se_2/NF catalysts, calculation of double-layer capacitance, characterization and activity of the catalysts, etc., are available in the online version of this paper.

Xuerong Zheng is a PhD student in the School of Materials Science and Engineering at Tianjin University. His recent research interest focuses on the development of electrochemical metallurgy methods for preparing micro/nanostructured materials for electrochemical and electrocatalysis applications.

Yida Deng is a Professor in the School of Materials Science and Engineering, Tianjin University. He received his PhD degree from Shanghai Jiao Tong University in 2006. His research interest includes metal and metal oxide nanostructures for electrochemical and energy applications.

Pt嵌入Ni_3Se_2@NiOOH核壳结构作为双功能催化剂提高全解水性能

郑学荣[1], 曹晏辉[1], 韩晓鹏[1], 刘辉[2], 王吉会[1], 张志佳[3], 吴贤文[4], 钟澄[1], 胡文彬[1], 邓意达[1*]

摘要 制备具有高效氢析出和氧析出双功能的电催化剂对提高大规模电解水制氢效率至关重要. 迄今为止, 无论是贵金属还是过渡金属化合物都未能达到令人满意的效果. 本文采用原位化学反应法制备了三维枝状Pt-Ni_3Se_2@NiOOH/NF(PNOF)纳米阵列. 泡沫镍作为镍源可有效减少界面电阻的影响, 表面NiOOH含有大量氧空位, 这些有效措施使PNOF催化剂同时具有优异的氢析出和氧析出性能. 同时作为电解水制氢的阴极和阳极, PNOF催化剂全解水电位在1.52 V即可实现10 mA cm^{-2}的电流密度, 并具有良好的稳定性. 这项工作为开发新型全解水催化剂提供了一种有效的方法.

